Supplementary Information

Measurement

Optical density at 600 nm (OD_{600}) was measured using a WPA CO8000 Cell Density Meter (Biochrom Ltd., Cambridge, UK). For reactions in microplates, absorbance was measured using a TECAN Infinite M200 PRO Multimode Microplate Reader (Tecan Ltd., Männedorf, Switzerland). Ultraviolet-visible spectra were recorded using a Shimadzu UV-2600 spectrophotometer and a Shimadzu UV-2450 spectrophotometer. ESI-TOF MS spectra were measured on a micrOTOF II (Bruker Daltonics). GC-MS analysis was performed using a Shimadzu GCMS-QP2010SE equipped with a Rtx-1 column (60 m × 0.32 mm; Restek corporation, Bellefonte, PA, USA). HPLC analysis was carried out using a Shimadzu HPLC system consisting of an SCL-10Avp system controller, LC-20AD pumps, DGU-$20A_3$ degasser, SIL-20A autosampler, CTO10-Avp column oven, SPD-10AVvp UV/Vis detector, equipped with an InertSustain AQ-C18 column (5 µm, 4.6 mm × 250 mm; GL Sciences Inc., Tokyo, Japan) or a COSMOSIL $5C_{18}$-MS-II packed column (4.6 mm I.D. × 250 mm; Nacalai Tesque, Inc., Kyoto, Japan)

General procedures for cell preparation

All bacterial type strains were inoculated into appropriate growth media in Erlenmeyer flasks. Cultures were incubated at their optimal growth temperatures with shaking for the respective durations (Table S1). After incubation, the cells were harvested and resuspended in phosphate buffer (87 mM Na_2HPO_4, 16 mM KH_2PO_4, 7 mM $MgSO_4$, 86 mM NaCl, 0.1 mM $CaCl_2$, pH 7.4), which served as a solvent for the subsequent reactions. Cell density was adjusted based on OD_{600}, except for *Streptomyces avermitilis* JCM 5070^T, *Actinosynnema pretiosum* subsp. *auranticum* JCM 7343^T, and *Saccharopolyspora erythraea* JCM 4748^T for which wet cell weight (WCW) was used instead.

Microtiter plate-based screening with a colorimetric assay

Benzene hydroxylation reactions were performed in 96-well microplates with a total mixture volume of 200 µL. Each reaction mixture contained bacterial cells (OD_{600} = 6.3 or WCW = 22.5g L^{-1}), decoy molecule (100 µM), glucose (40 mM), DMSO (1.5% [v/v]), and benzene (10 mM) in the phosphate buffer. The microplates were sealed with an aluminum seal and incubated at 25 °C and 1700 rpm for 4 h on a plate shaker (Biomixer PMA-001, Biotec). After incubation, the microplates were centrifuged at 3700 rpm for 10 min, and 100 µL of the supernatant was transferred to new microplates. To each well, 15 µL of 4-aminoantiyrine solution (5 mg mL^{-1}, aqueous) and 15 µL of $K_2S_2O_8$ solution (5 mg mL^{-1}, aqueous) were added.[1-2] After 30 min, absorbance at 509 nm was measured to quantify phenol formation.

GC-MS and HPLC analytical procedures for hydroxylation reactions

General procedure for hydroxylation reactions

Each reaction mixture (1 mL) in a 6 mL vial contained bacterial cells (OD_{600} = 6.3), decoy molecule (100 µM), glucose (40 mM), DMSO (1.5% [v/v]), and a substrate in the phosphate buffer. The vials were incubated at designated temperatures with shaking at 180 rpm. The uncertainty is given as the standard deviation of at least three independent experiments.

For benzene hydroxylation

After the reaction, 500 μL of the reaction mixture was extracted with 500 μL of dichloromethane, to which 10 μL of 40 mM indane (in DMSO) was added as an internal standard. The organic phase was separated and directly subjected to GC-MS analysis. The GC-MS analytical conditions were as follows: column temperature program, 40 °C for 2 min, then 20 °C min^{-1} to 200 °C and held for 5 min; injection temperature, 240 °C; interface temperature, 200 °C; ion source temperature, 200 °C; carrier gas, helium; flow rate, 3.11 mL min^{-1}; split mode, split ratio 10:1.

For toluene and fluorobenzene hydroxylations

After the reaction, 500 μL of the reaction mixture was extracted with 500 μL of dichloromethane, to which 10 μL of 100 mM phenol (in DMSO) was added as an internal standard. The organic phase was separated and directly subjected to GC-MS analysis. The GC-MS analytical conditions were as follows: column temperature program, 140 °C for 20 min, then 10 °C min^{-1} to 200 °C; injection temperature, 250 °C; interface temperature, 200 °C; ion source temperature, 200 °C; carrier gas, helium; flow rate, 2.83 mL min^{-1}; split mode, split ratio 10:1.

For *o*-xylene and *p*-xylene hydroxylations

After the reaction, 500 μL of the reaction mixture was extracted with 500 μL of dichloromethane, to which 10 μL of 40 mM indane (in DMSO) was added as an internal standard. The organic phase was separated and directly subjected to GC-MS analysis. The GC-MS analytical conditions were as follows: column temperature program, 140 °C for 20 min, then 10 °C min^{-1} to 200 °C and held for 3 min; injection temperature, 250 °C; interface temperature, 200 °C; ion source temperature, 200 °C; carrier gas, helium; flow rate, 2.83 mL min^{-1}; split mode, split ratio 10:1.

For *m*-xylene hydroxylation

After the reaction, 500 μL of the reaction mixture was extracted with 500 μL of dichloromethane, to which 10 μL of 40 mM indane (in DMSO) was added as an internal standard. The organic phase was separated and directly subjected to GC-MS analysis. The GC-MS analytical conditions were as follows: column temperature program, 140 °C for 20 min, then 10 °C min^{-1} to 200 °C; injection temperature, 250 °C; interface temperature, 200 °C; ion source temperature, 200 °C; carrier gas, helium; flow rate, 2.83 mL min^{-1}; split mode, split ratio 10:1.

For chlorobenzene hydroxylation

After the reaction, 500 μL of the reaction mixture was extracted with 500 μL of dichloromethane, to which 10 μL of 100 mM phenol (in DMSO) was added as an internal standard. The organic phase was separated and directly subjected to GC-MS analysis. The GC-MS analytical conditions were as follows: column temperature program, 140 °C for 20 min, then 10 °C min^{-1} to 200 °C and held for 4 min; injection temperature, 250 °C; interface temperature, 200 °C; ion source temperature, 200 °C; carrier gas, helium; flow rate, 2.83 mL min^{-1}; split mode, split ratio 10:1.

For naphthalene

After the reaction, 500 μL of the reaction mixture was quenched by adding 500 μL of acetonitrile. The resulting

supernatant was filtered through a 0.20 μm PVDF SEPARA® syringe-less filter (GVS S.p.A, Italy) and directly subjected to reversed-phase HPLC analysis. The HPLC analytical conditions were as follows: flow rate, 0.70 mL min^{-1}; mobile phase, water and acetonitrile, both containing 0.1% trifluoroacetic acid (TFA); gradient program, 45% acetonitrile for 15 min, then increased at 5% min^{-1} to 95% and held for 20 min; column temperature, 40 °C; detection wavelength, 271 nm.

Hydroxylation reaction under a mixed-substrate condition

Each reaction mixture (1 mL) in a 6 mL vial contained bacterial cells (OD_{600} = 6.3), decoy molecule (100 μM), glucose (40 mM), DMSO (1.5% [v/v]), and substrate (benzene, toluene, and *o*-xylene; 1 mM each) in the phosphate buffer. After incubation at 45 °C with shaking at 180 rpm for 4 h, 500 μL of the reaction mixture was extracted with 500 μL of dichloromethane, to which 10 μL of 20 mM 1-indanol (in DMSO) was added as an internal standard. The organic phase was separated and directly subjected to GC-MS analysis. The GC-MS analytical conditions were as follows: column temperature program, 140 °C for 20 min, then 10 °C min^{-1} to 200 °C and held for 4 min; injection temperature, 250 °C; interface temperature, 200 °C; ion source temperature, 200 °C; carrier gas, helium; flow rate, 2.83 mL min^{-1}; split mode, split ratio 10:1.

Degradation of mono-chlorinated dibenzo-*p*-dioxins (1- and 2-CDDs)

Degradation of mono-chlorinated dibenzo-*p*-dioxins was determined using separate vials prepared for each time point. Each reaction mixture (1 mL) in a 6 mL vial contained bacterial cells (OD_{600} = 6.3), decoy molecule (100 μM), glucose (40 mM), DMSO (1.5% [v/v]), and mono-chlorinated dibenzo-*p*-dioxin (1- or 2-CDD, 10 μM) in the phosphate buffer. The vials were incubated at 30 °C for *P. megaterium* and at 45 °C for *B. subtilis* with shaking at 180 rpm. At each designated time point, the reaction was quenched by adding 500 μL of acetonitrile, to which 10 μL of 50 mM *p*-nitrophenol (in DMSO) was also added as an internal standard. The resulting supernatant was filtered through a 0.20 μm PVDF SEPARA® syringe-less filter (GVS S.p.A, Italy) and directly subjected to reversed-phase HPLC analysis. The HPLC analytical conditions were as follows: flow rate, 0.50 mL min^{-1}; mobile phase, water and acetonitrile, both containing 0.1% TFA; gradient program, 40% to 100% at 3% min^{-1}, followed by holding at 100% for 20 min; column temperature, 40 °C; detection wavelength, 295 nm.

Degradation of dibenzo-*p*-dioxin (DD) was carried out similarly, except that the initial substrate concentration was 500 μM and different HPLC analytical conditions were used: flow rate, 0.50 mL min^{-1}; mobile phase, water and acetonitrile, both containing 0.1% TFA; gradient program, 45% to 95% at 5% min^{-1}, followed by holding at 95% for 20 min; column temperature, 40 °C; detection wavelength, 289 nm.

Product identification in DD degradation

The reaction mixture (10 mL) in a 50 mL vial contained *B. subtilis* JCM 1465^T (OD_{600} = 6.3), (*S*)-Ibu-Leu (100 μM), glucose (40 mM), DMSO (1.5% [v/v]), and DD (500 μM) in the phosphate buffer. The vial was incubated at 45 °C and 180 rpm for 3 h. After incubation, the reaction mixture was extracted with 20 mL of dichloromethane, and the organic phase was evaporated to dryness and reconstituted in 200 μL of solvent.

The solution was then treated with sodium sulfate to remove residual water, and the resulting solution was derivatized

with BSTFA-TMCS (99:1) for 30 min at room temperature prior to GC-MS analysis. The GC-MS analytical conditions were as follows: column temperature program, 80 °C to 250 °C at 10 °C min^{-1}, followed by holding at 250 °C for 133 min; injection temperature, 250 °C; interface temperature, 200 °C; ion source temperature, 200 °C; carrier gas, helium; flow rate, 2.98 mL min^{-1}; split mode, split ratio 10:1.

Reactions using *Escherichia coli* BL21(DE3) overexpressing P450 enzymes

1. Construction of expression vectors

Full-length wild-type CYP102A1 (P450BM3)

A sequence of full-length CYP102A1 was introduced into the pET28a(+) vector as previously described.[3]

Full-length wild-type CYP102A2 and CYP102A3

B. subtilis JCM 1465^T genome was extracted using a NucleoSpin® Microbial DNA Kit (Macherey-Nagel). The full-length CYP102A2 and CYP102A3 genes were subsequently amplified by PCR using the extracted genome as the template with the following primers, respectively.

> For CYP102A2

FP: 5'- GGCAGCCATATGGCTAGCATGAAGGAAACAAGCCCGATTC -3'

RP: 5'- TCCACCAGTCATGCTAGCCTATATCCCTGCCCAGACATCC -3'

> For CYP102A3

FP: 5'- CAGCCATATGGCTAGCATGAAACAGGCAAGCGCAATACC -3'

RP: 5'- CACCAGTCATGCTAGCTTACATTCCTGTCCAAACGTCTTTC -3'

Each amplicon was separated by agarose gel electrophoresis followed by gel extraction. The resulting fragment was ligated into the pET28a(+) vector, linearized with NheI, following the instructions provided in the In-Fusion® HD Cloning Kit (Takara Bio). The constructed vector was transformed into competent *E. coli* DH5α cells, and the correct insertion of the target gene was confirmed by sequencing. For protein overexpression, the constructed vector was transformed into *E. coli* BL21(DE3).

2. Cultivation, protein expression, and cell preparation for whole-cell hydroxylation

E. coli BL21(DE3) transformed with the pET28a-P450 vector described above was inoculated into Luria-Bertani (LB) medium in an Erlenmeyer flask and incubated at 37 °C with shaking at 180 rpm. 5-Aminolevulinic acid (0.5 mM) and isopropyl-β-D-1-thiogalactopyranoside (IPTG, 0.1 mM) were added when the OD_{600} reached 0.4–0.6 and 0.8–0.9, respectively. The culture was subsequently incubated at 25 °C with shaking at 150 rpm for 19 h to express the P450 enzyme. After harvesting and resuspending the cells in the phosphate buffer, benzene hydroxylation was carried out following the experimental procedure described above.

Reactions using gene-knockout mutants

B. subtilis JCM 1465^{T} possesses two CYP102 family enzymes, which are identical to those of *B. subtilis* strain 168 according to a previous whole-genome sequencing study.[4] Gene-knockout mutants of strain 168, constructed in the previous report,[5] were provided by National BioResource Project (NIG, Japan): B. subtilis. Each gene was disrupted by replacement with an erythromycin resistance cassette (Erm^{R}).

B. subtilis strain 168 WT (MGNA-A001), Δ*cyp102a2* (BKE07250), and Δ*cyp102a3* (BKE27160) were inoculated into LB medium in Erlenmeyer flasks, with erythromycin (1 μg mL^{-1}) added for the knockout strains. Cultures were incubated at 30 °C with shaking for 20 h, after which the cells were harvested and resuspended in the phosphate buffer. Benzene hydroxylation and DD degradation were then carried out following the experimental procedures described above.

Modeling of protein-ligand complexes of CYP102A2 and CYP102A3

1. AlphaFold2 models as initial structures

AlphaFold2[6]-predicted structures of CYP102A2 (O08394) and CYP102A3 (O08336) were downloaded from the AlphaFold Protein Structure Database (https://alphafold.ebi.ac.uk/) and truncated at Ala457 to include only the heme domains, based on amino acid sequence alignment with CYP102A1 using Clustal Omega[7]. Since the structures do not include cofactors, the heme b was subsequently inserted by structural alignment with a crystal structure of CYP102A1 (PDB: 3WSP).

2. Molecular dynamics (MD) simulations for structural refinement of the modeled structures

The protonation states of the structures at pH 7.4 were estimated using PROPKA[8] implemented in Maestro (Schrödinger Release 2023-4; Schrödinger, LLC, New York, NY, USA). The force field parameters and atomic partial charges of the penta-coordinated ferric high-spin heme and its coordinating cysteine ligand were derived from the literature.[9]

Each structure was solvated in a box of TIP3P water molecules[10] with a 10 Å buffer and neutralized by the addition of sodium cations using the LEaP module in AmberTools23.[11] The ff14SB[12] and GAFF2[13] force fields were applied to protein and non-protein solutes, respectively. The resulting topology files were then converted into GROMACS format using ParmEd.[14] MD simulations were performed using GROMACS 2024.2.[15] Energy minimization using the steepest descent method was performed in two steps: first with a restrained potential of 1000 kJ mol^{-1} nm^{-2} applied to the protein heavy atoms, followed by an unrestrained step. The systems were then heated to 300K in the NVT ensemble for 200ps, during which harmonic position restraints of 1000 kJ mol^{-1} nm^{-2} were applied to the protein heavy atoms. Next, the systems were equilibrated to 300K and 1 bar in the NPT ensemble, with the position restraints gradually reduced from 1000 kJ mol^{-1} nm^{-2} to 10 kJ mol^{-1} nm^{-2} over seven consecutive 1-ns steps. Temperature and pressure were maintained using the v-rescale thermostat[16] and c-rescale barostat[17], respectively. Finally, 50-ns production runs with a 2-fs time step were performed in the NPT ensemble using the Parrinello-Rahman barostat.[18] Long-range electrostatics were treated using the Particle Mesh Ewald (PME) method,[19] and the cutoff distance for non-bonded interactions was set to 1.0 nm. The P-LINCS algorithm[20] was used to constrain the bonds involving hydrogen atoms. Coordinates during each simulation were saved every 1.0 ps. Three independent simulations with different initial velocities (150 ns in total) were performed for extensive conformational sampling.

The MD trajectories were post-processed using *trjconv* in GROMACS. The last 40 ns of each of the three trajectories were combined, and the most average-like structure was extracted from the combined trajectories based on the root mean square deviation of all Cα atoms.

3. Docking simulations using AutoDock Vina

AutoDock Vina v1.1.2[21] was used for all docking experiments. The substrate (1- or 2-CDD) and the decoy molecule ((*S*)-Ibu-Leu) were docked stepwise to the extracted average structures. For the substrate, the search space was defined above the heme with a box size of 15 × 15 × 15 $Å^3$, and the best-scoring pose was selected as the receptor for subsequent docking of the decoy molecule. The decoy molecule, (*S*)-Ibu-Leu, was then docked into a larger box encompassing the entire cavity, with a box size of 22.5 × 22.5 × 30 $Å^3$. The *exhaustiveness* parameter was set to 16 for all simulations. Finally, protein-ligand interactions in the top-ranked docking poses were analyzed and visualized using the Protein-Ligand Interaction Profiler (PLIP, v2.3.1).[22]

Table S1. Growth conditions for each strain.

Strains	JCM	ATCC	Culture medium No.[a] / Growth temperature [°C]	Incubation time
Priestia megaterium	2506^T	14581	No. 22 / 30 °C	20 h
Bacillus subtilis subsp. *subtilis*	1465^T	6051	No. 22 / 30 °C	20 h
Bacillus cereus	2152^T	14579	No. 22 / 30 °C	20 h
Bacillus licheniformis	2505^T	14580	No. 22 / 37 °C	20 h
Bacillus thuringiensis	20386^T	10792	No. 22 / 30 °C	20 h
Bacillus pumilus	2508^T	7061	No. 22 / 30 °C	20 h
Streptomyces avermitilis	5070^T	31267	No. 42 / 28 °C	5 days
Rhodococcus erythropolis	3201^T	25544, 4277	No. 43 / 28 °C	3 days
Actinosynnema pretiosum subsp. *auranticum*	7343^T	31309	No. 43 / 28 °C	5 days
Saccharopolyspora erythraea	4748^T	11635	No. 42 / 28 °C	5 days

[a] Culture media composition as published by Japan Collection of Microorganisms (JCM):

- No. 22: 10.0 g L^{-1} meat peptone, 10.0 g L^{-1} beef extract, 5.0 g L^{-1} NaCl, pH 7.0
- No. 42: 2.0 g L^{-1} yeast extract, 10.0 g L^{-1} soluble starch, pH 7.3
- No. 43: 4.0 g L^{-1} yeast extract, 10.0 g L^{-1} malt extract, 4.0 g L^{-1} glucose, pH 7.3

Table S2. Percent identity matrix of the heme domains of CYP102 family enzymes. Sequences of CYP102A1 to G2 were obtained from the Cytochrome P450 Homepage[23] and aligned using Clustal Omega[7].

	(%)	A1	A2	A3	A5	A7	A8	A15	B2	C2	D1	F1	G2
CYP102	A1	100	64.7	65.8	66.3	65.9	65.4	60.3	43.2	40.9	42.2	46.3	46.2
	A2		100	67.8	79.9	70.4	81.6	63.9	41.4	42.6	44.4	46.2	45.5
	A3			100	67.3	74.5	66.6	68.4	44.0	42.1	43.6	48.8	46.1
	A5				100	70.0	96.8	64.5	42.4	42.9	45.5	45.4	46.1
	A7					100	69.8	68.9	44.7	43.4	42.5	47.9	46.1
	A8						100	64.5	43.0	43.6	45.9	45.8	45.8
	A15							100	41.3	41.7	43.7	45.6	45.3
	B2								100	47.8	38.1	43.8	50.9
	C2									100	40.0	41.2	45.6
	D1										100	39.1	39.7
	F1											100	45.0
	G2												100

Table S3. Six genes annotated as cytochrome P450s in the *P. megaterium* JCM 2506^T (ATCC 14581^T) genome (based on NCBI RefSeq annotation). The most closely related P450s for each gene were identified using P450Atlas[24].

NCBI RefSeq assembly	Locus tag	Best-matched P450 in P450Atlas (AA sequence identity, %)	AA sequence identity to full-length CYP102A1 (Clustal Omega[7])
GCF_000832985.1	BG04_163	CYP102A1 (100.0%)	100.0%
	BG04_798	CYP109E1 (98.02%)	20.60%
	BG04_4190	CYP106A1 (100.0%)	18.60%
	BG04_4340	CYP1756A1 (96.49%)	22.02%
	BG04_4382	CYP109A2 (100.0%)	17.63%
	BG04_5610	CYP152K5 (100.0%)	14.39%

Table S4. Eight P450s in the genomes of *B. subtilis* JCM 1465^T (ATCC 6051^T) and strain 168. The corresponding genes in the strains showed complete identity in both nucleotide and amino acid sequences. The most closely related P450s were identified using P450Atlas[24].

	Strain NCBI RefSeq assembly		Gene name	Best-matched P450 in P450Atlas (AA sequence identity, %)	AA sequence identity to full-length CYP102A1 (Clustal Omega[7])
	JCM 1465^T (ATCC 6051^T) GCF_000344745.1	Strain 168 GCF_000009045.1			
Locus tag	BSU6051_02100	BSU02100	*cypC*	CYP152A1 (96.16%)	15.43%
	BSU6051_07250	BSU07250	*yetO*	CYP102A2 (100.0%)	59.06%
	BSU6051_12210	BSU12210	*yjiB*	CYP109B1 (98.99%)	20.22%
	BSU6051_17230	BSU17230	*pksS*	CYP107K1 (99.01%)	19.73%
	BSU6051_26740	BSU26740	*cypA*	CYP107J1 (96.34%)	17.43%
	BSU6051_27160	BSU27160	*cypB*	CYP102A3 (100.0%)	58.30%
	BSU6051_30190	BSU30190	*bioI*	CYP107H1 (97.72%)	18.06%
	BSU6051_35060	BSU35060	*cypX*	CYP134A1 (99.75%)	16.71%

Table S5. Environmental fate predictions obtained from OPERA[25] for five decoy molecules and representative aromatic pollutants. Ready biodegradability, fish biotransformation half-life (KM), and soil adsorption coefficient (KOC) were predicted.

	Compound	Ready Biodegradability			log KM			log KOC		
		Predicted[a]	AD[b]	CLI[c]	Predicted	AD	CLI	Predicted	AD	CLI
Decoy	C7-Pro-Phe	1	1	0.48	– 0.78	1	0.49	3.34	1	0.52
	(*S*)-Ibu-Phe	0	1	0.59	– 0.74	1	0.50	4.17	1	0.51
	(*S*)-Ibu-Leu	0	1	0.51	– 0.4	1	0.45	3.15	1	0.51
	PFC9-Ala	0	0	0.65	0.32	0	0.11	4.14	0	0.25
	C10-Phe	1	1	0.54	– 0.69	1	0.51	3.56	1	0.45
Pollutant	Benzene	1	1	0.79	– 1.07	1	0.70	1.75	1	0.93
	toluene	1	1	0.67	– 0.63	1	0.58	2.07	1	0.93
	Naphthalene	0	1	0.61	0.41	1	0.86	2.96	1	0.98
	DD	1	1	0.56	0.19	1	0.40	4.3	1	0.75
	1-CDD	1	1	0.55	0.44	1	0.42	4.31	1	0.74
	2-CDD	1	1	0.54	0.45	1	0.44	4.51	1	0.74

[a] Predicted values obtained using OPERA v2.9.2. [b] AD: applicability domain. A value of 1 indicates that the compound is within the applicability domain of the OPERA model. [c] CLI: confidence level index.

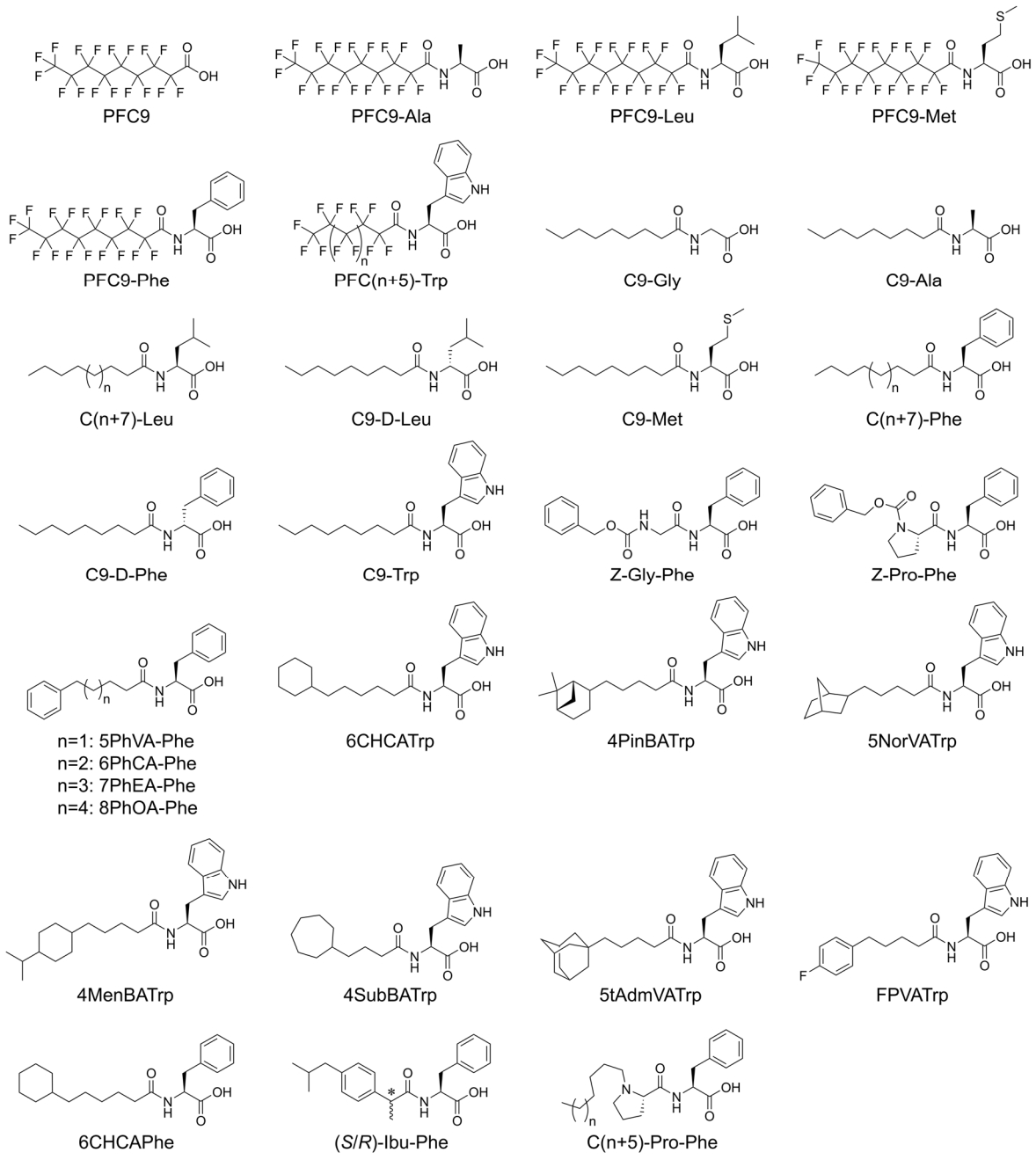

Fig. S1. Chemical structures of decoy molecules used in this study (continued on the next page).

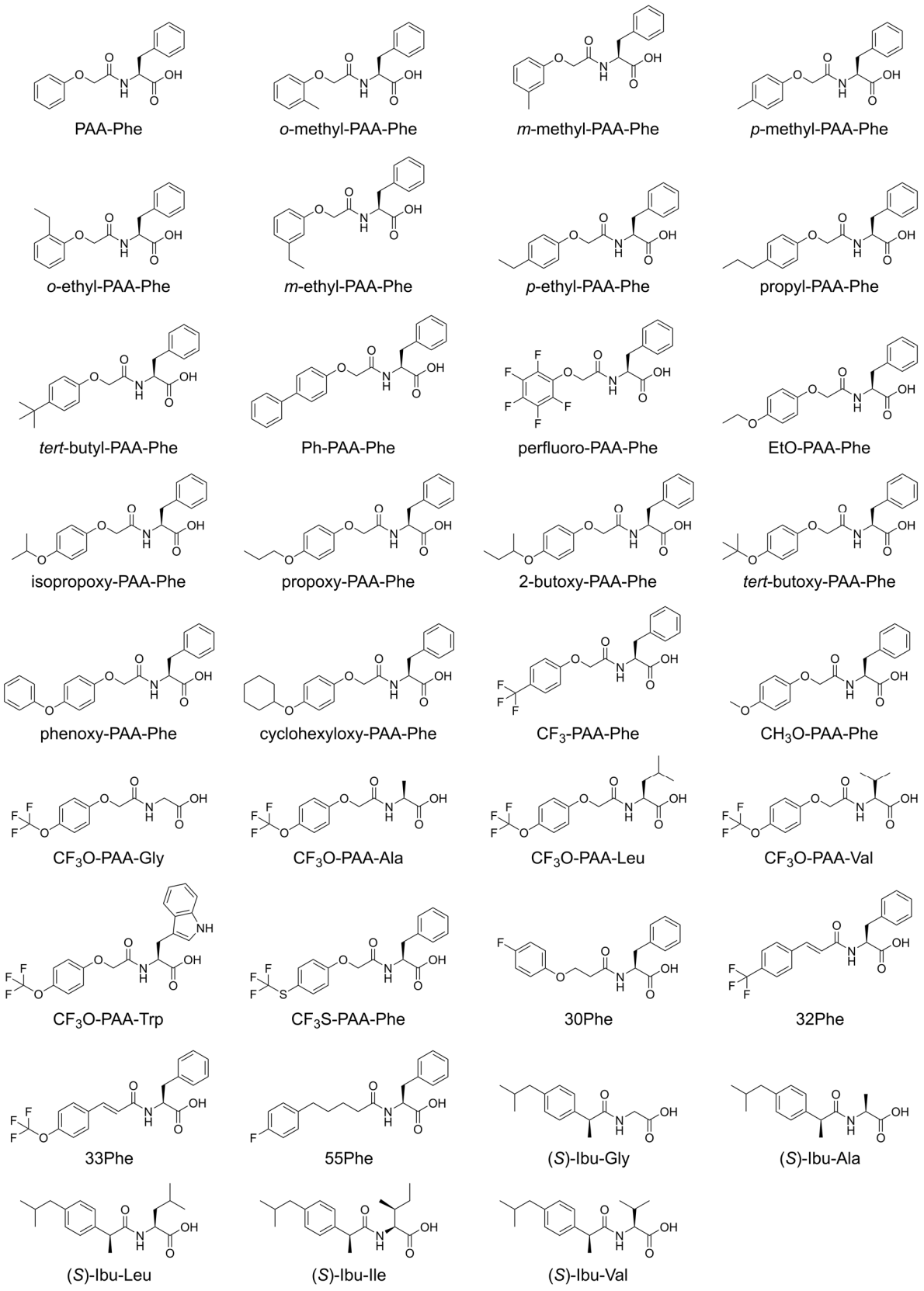

Fig. S1. (continued).

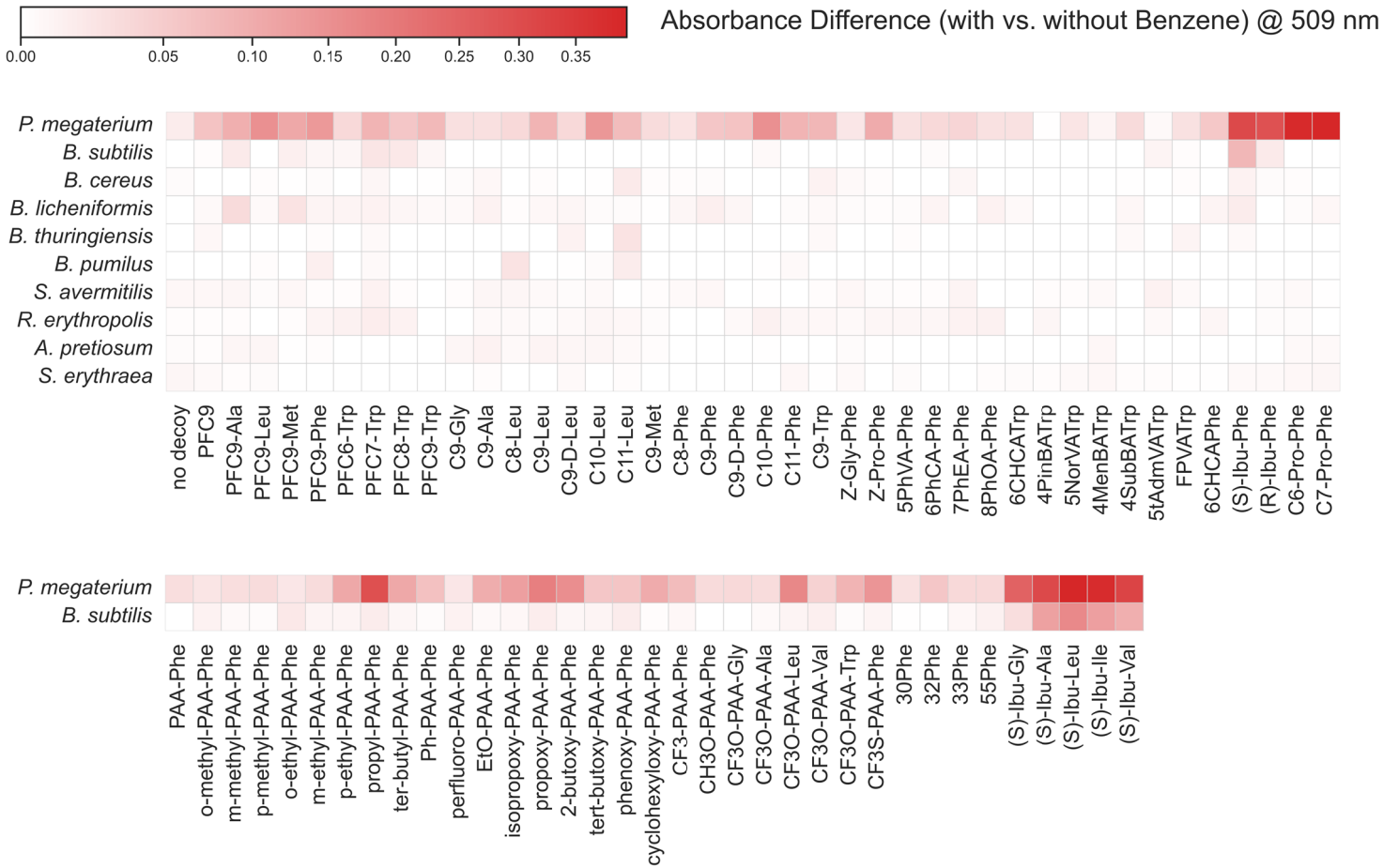

Fig. S2. Microplate-based screening of bacterium-decoy molecule combinations for benzene hydroxylation. Each reaction mixture contained bacterial cells (OD_{600} = 6.3 or WCW = 22.5 g L^{-1}), decoy molecule (100 μM), glucose (40 mM), DMSO (1.5% [v/v]), and benzene (10 mM) in the phosphate buffer, with a total reaction volume of 200 μL. After incubation at 25 °C with shaking at 1700 rpm for 4 h, phenol formation was quantified via a colorimetric assay using 4-aminoantipyrine. Each value represents the mean of three independent experiments. The heatmap shows absorbance differences between benzene-present and benzene-absent conditions. A mild power-law normalization (matplotlib's PowerNorm, $\gamma = 0.7$) was applied to enhance the visibility of small positive differences.

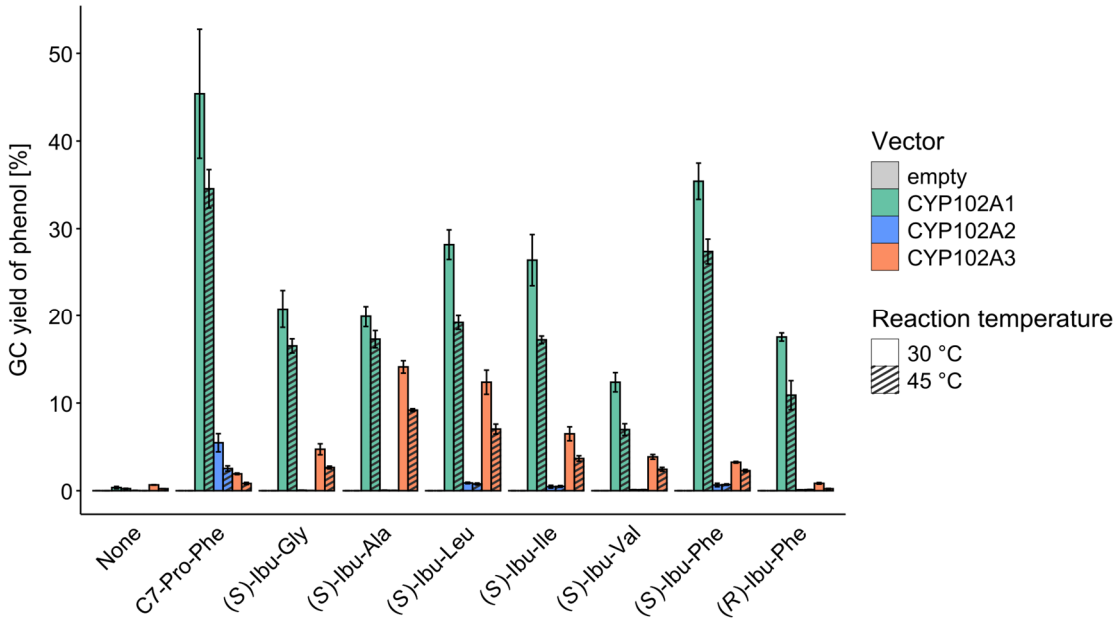

Fig. S3. Benzene hydroxylation using *E. coli* BL21(DE3) expressing each P450. Reactions were carried out in 6 mL vials containing bacterial cells (OD_{600} = 6.3), decoy molecule (100 μM), glucose (40 mM), DMSO (1.5% [v/v]), and benzene (10 mM) in the phosphate buffer, with a total reaction volume of 1 mL. After incubation at the designated temperature with shaking at 180 rpm for 4 h, phenol formation was quantified by GC-MS analysis. Values represent the mean ± standard deviation of three independent biological replicates derived from different cell culture batches.

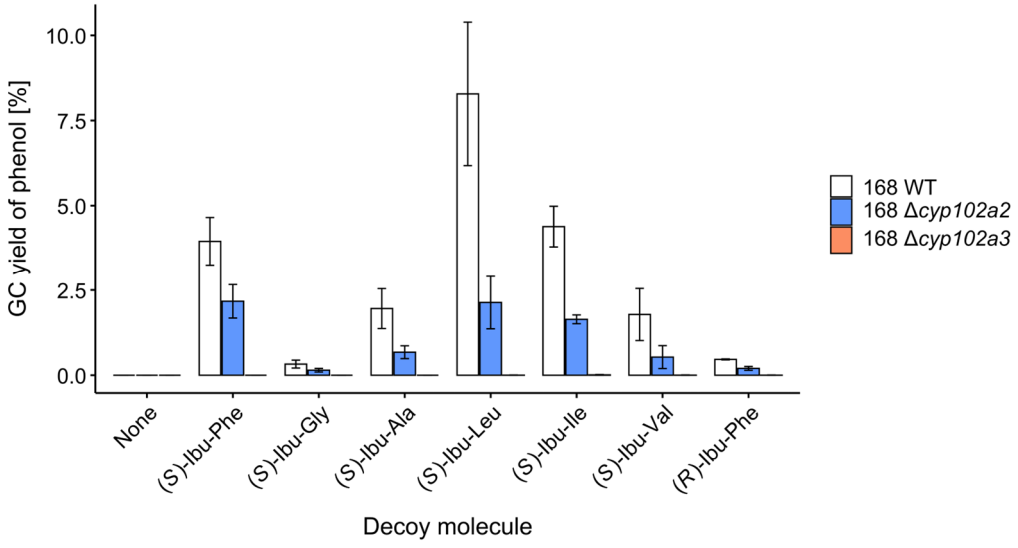

Fig. S4. Benzene hydroxylation by *B. subtilis* 168 and its gene-knockout mutants. Reactions were carried out in 6 mL vials containing bacterial cells (OD_{600} = 6.3), decoy molecule (100 μM), glucose (40 mM), DMSO (1.5% [v/v]), and benzene (10 mM) in the phosphate buffer, with a total reaction volume of 1 mL. After incubation at 45 °C with shaking at 180 rpm for 4 h, phenol formation was quantified by GC-MS analysis. Values represent the mean ± standard deviation of three independent biological replicates derived from different cell culture batches.

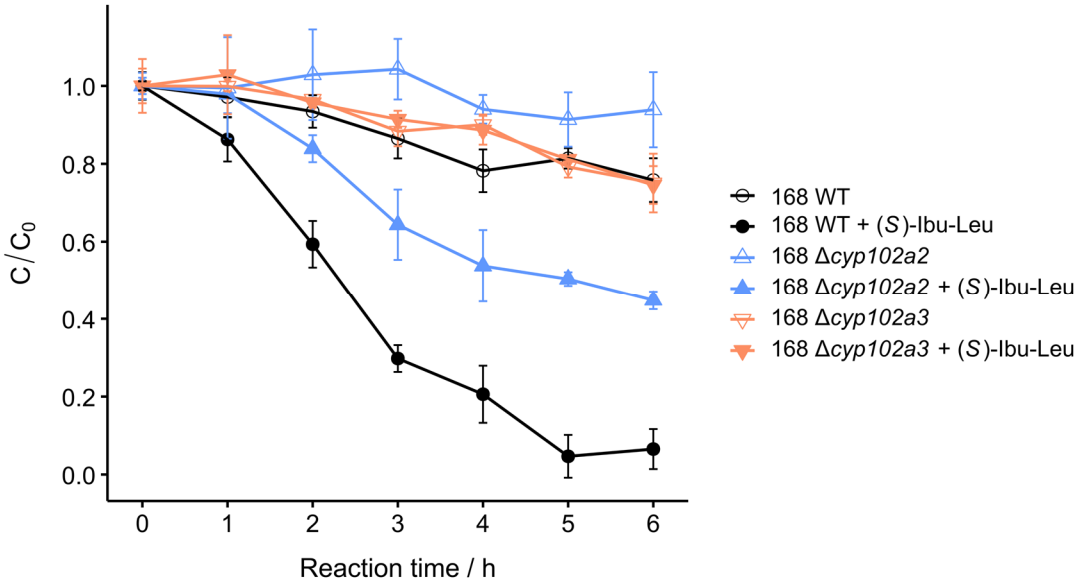

Fig. S5. Dibenzo-*p*-dioxin degradation using *B. subtilis* 168 WT and gene-knockout mutants. Reactions were carried out in 6 mL vials containing bacterial cells (OD_{600} = 6.3), decoy molecule (100 µM), glucose (40 mM), DMSO (1.5% [v/v]), and DD (500 µM) in the phosphate buffer, with a total reaction volume of 1 mL. After incubation at 45 °C with shaking at 180 rpm for each time point, the residual amounts of DD were quantified by HPLC analysis. Values represent the mean ± standard deviation of three independent biological replicates derived from different cell culture batches.

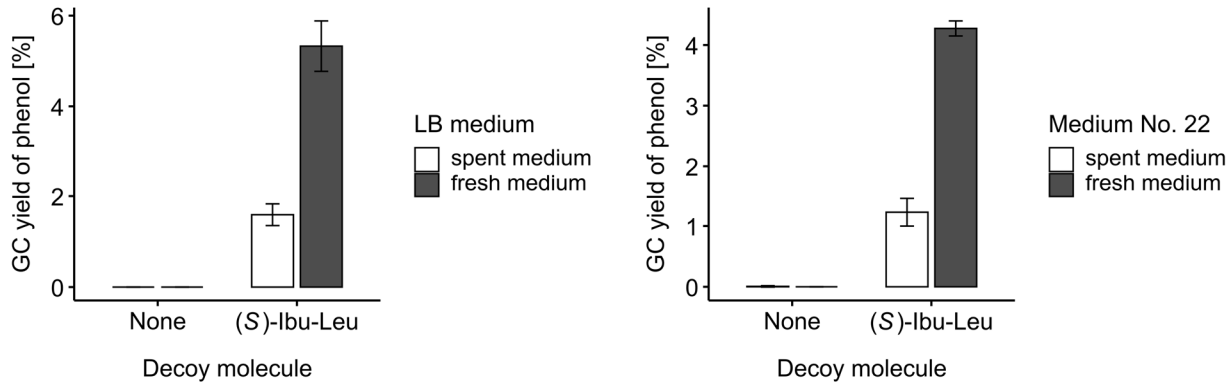

Fig. S6. Benzene hydroxylation by *B. subtilis* JCM 1465^T in growth media (left: LB medium; right: Medium No. 22). *B. subtilis* was inoculated into each growth medium and incubated at 30 °C with shaking for 20 h. For "spent medium", cells were left in the cultured medium in which the bacterium was grown. For "fresh medium", cells harvested from the cultured medium were resuspended in newly prepared medium before the reaction. Reactions were carried out in 6 mL vials by adding the following to the media: decoy molecule (100 µM), glucose (40 mM), DMSO (1.5% [v/v]), and benzene (10 mM), resulting in a total reaction volume of 1 mL. Initial cell densities during the reactions were as follows: LB medium—spent: OD_{600} = 4.6, fresh: OD_{600} = 5.3; Medium No. 22—spent: OD_{600} = 6.0, fresh: OD_{600} = 6.3. After incubation at 45 °C with shaking at 180 rpm for 4 h, phenol formation was quantified by GC-MS analysis. Values represent the mean ± standard deviation of three independent biological replicates derived from different cell culture batches.

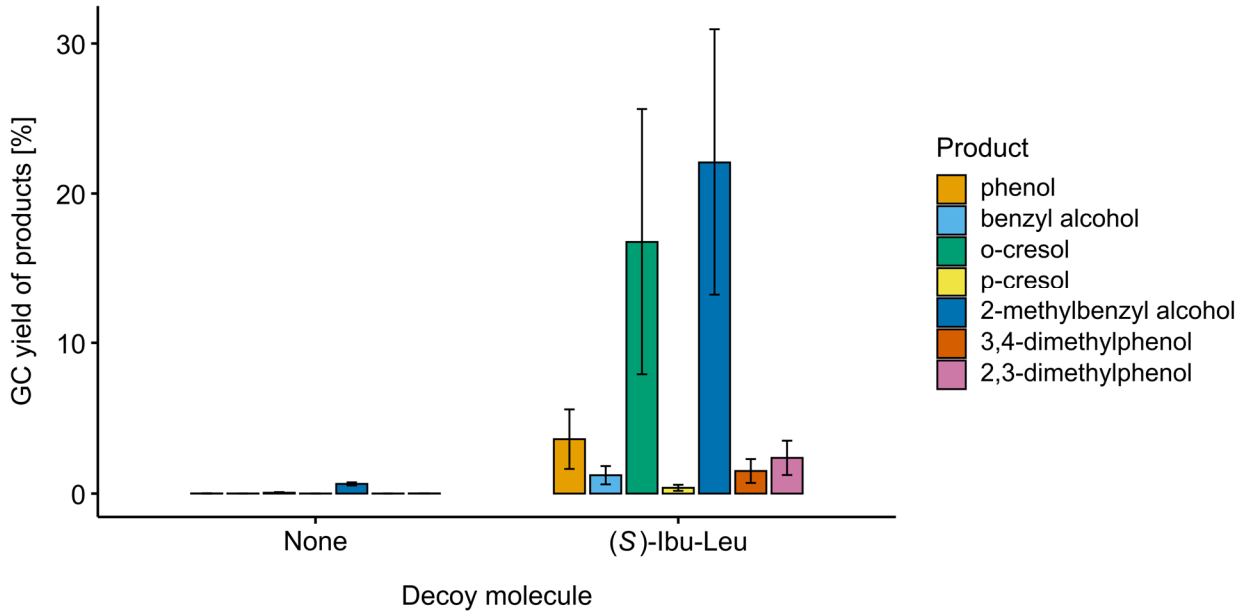

Fig. S7 Hydroxylation reaction under a mixed-substrate condition by *B. subtilis* JCM 1465^{T}. Reactions were carried out in 6 mL vials containing bacterial cells (OD_{600} = 6.3), decoy molecule (100 µM), glucose (40 mM), DMSO (1.5% [v/v]), and substrates (benzene, toluene, and *o*-xylene; 1 mM each) in the phosphate buffer, with a total reaction volume of 1 mL. After incubation at 45 °C with shaking at 180 rpm for 4 h, the products were quantified by GC-MS analysis. Values represent the mean ± standard deviation of three independent biological replicates derived from different cell culture batches.

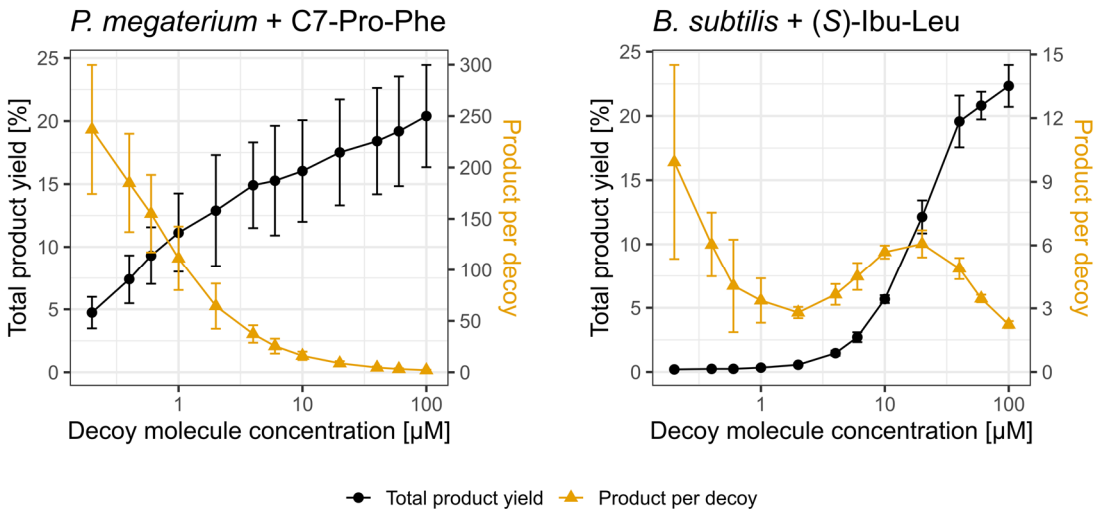

Fig. S8. Naphthalene hydroxylation with different decoy molecule concentrations. Reactions were carried out in 6 mL vials containing bacterial cells (OD_{600} = 6.3), decoy molecule, glucose (40 mM), DMSO (1.5% [v/v]), and naphthalene (1 mM) in the phosphate buffer, with a total reaction volume of 1 mL. After incubation at 45 °C with shaking at 180 rpm for 4 h, the products were quantified by HPLC analysis. Total product yield represents the combined HPLC yield of 1-naphthol and 2-naphthol. Product per decoy represents the total amount of hydroxylated products (1-naphthol + 2-naphthol) normalized to the concentration of the added decoy molecule. Values represent the mean ± standard deviation of three independent biological replicates derived from different cell culture batches. Left: *P. megaterium* with C7-Pro-Phe; right: *B. subtilis* with (*S*)-Ibu-Leu.

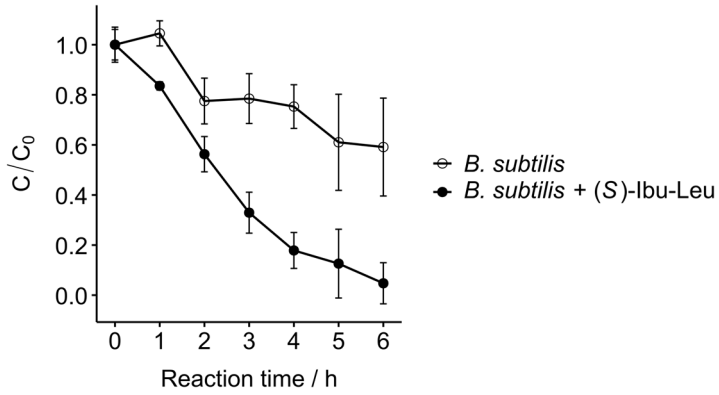

Fig. S9. Degradation of dibenzo-*p*-dioxin by *B. subtilis* JCM 1465^{T}. Reactions were carried out in 6 mL vials containing bacterial cells (OD_{600} = 6.3), decoy molecule (100 μM), glucose (40 mM), DMSO (1.5% [v/v]), and DD (500 μM) in the phosphate buffer, with a total reaction volume of 1 mL. After incubation at 45 °C with shaking at 180 rpm for each time point, the residual amounts of DD were quantified by HPLC analysis. Values represent the mean ± standard deviation of three independent biological replicates derived from different cell culture batches.

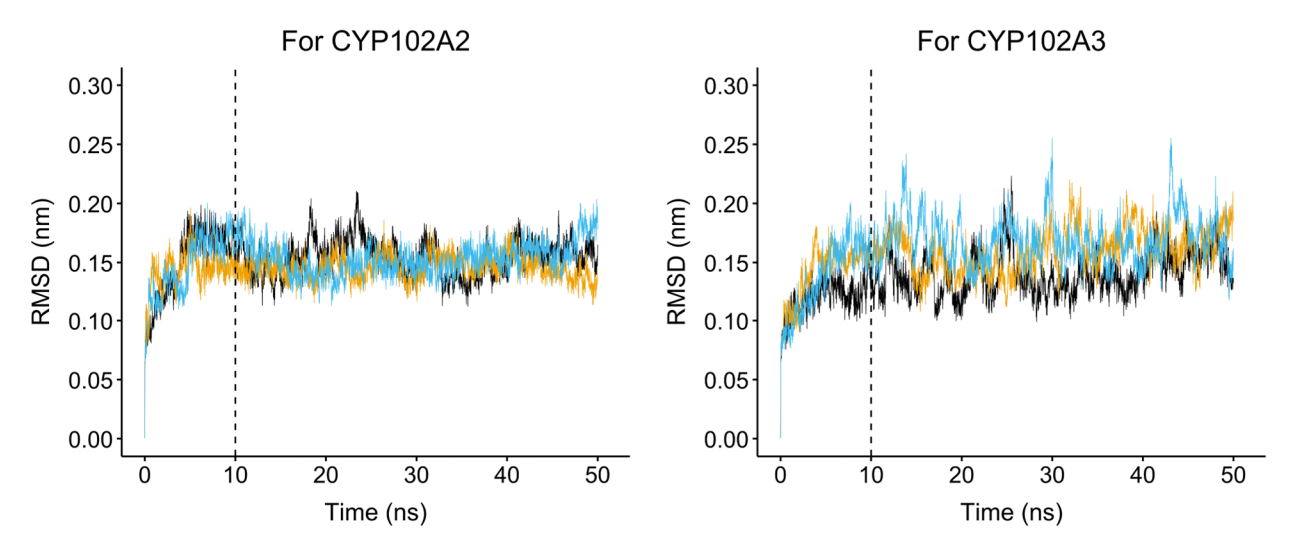

Fig. S10. RMSD profiles of the backbone atoms of CYP102A2 and CYP102A3 during three independent MD simulations each. RMSD was calculated for N, Cα, and C atoms using the initial structure as the reference. The last 40 ns of each 50-ns trajectory were combined, and the most average-like structure was extracted for subsequent docking simulations.

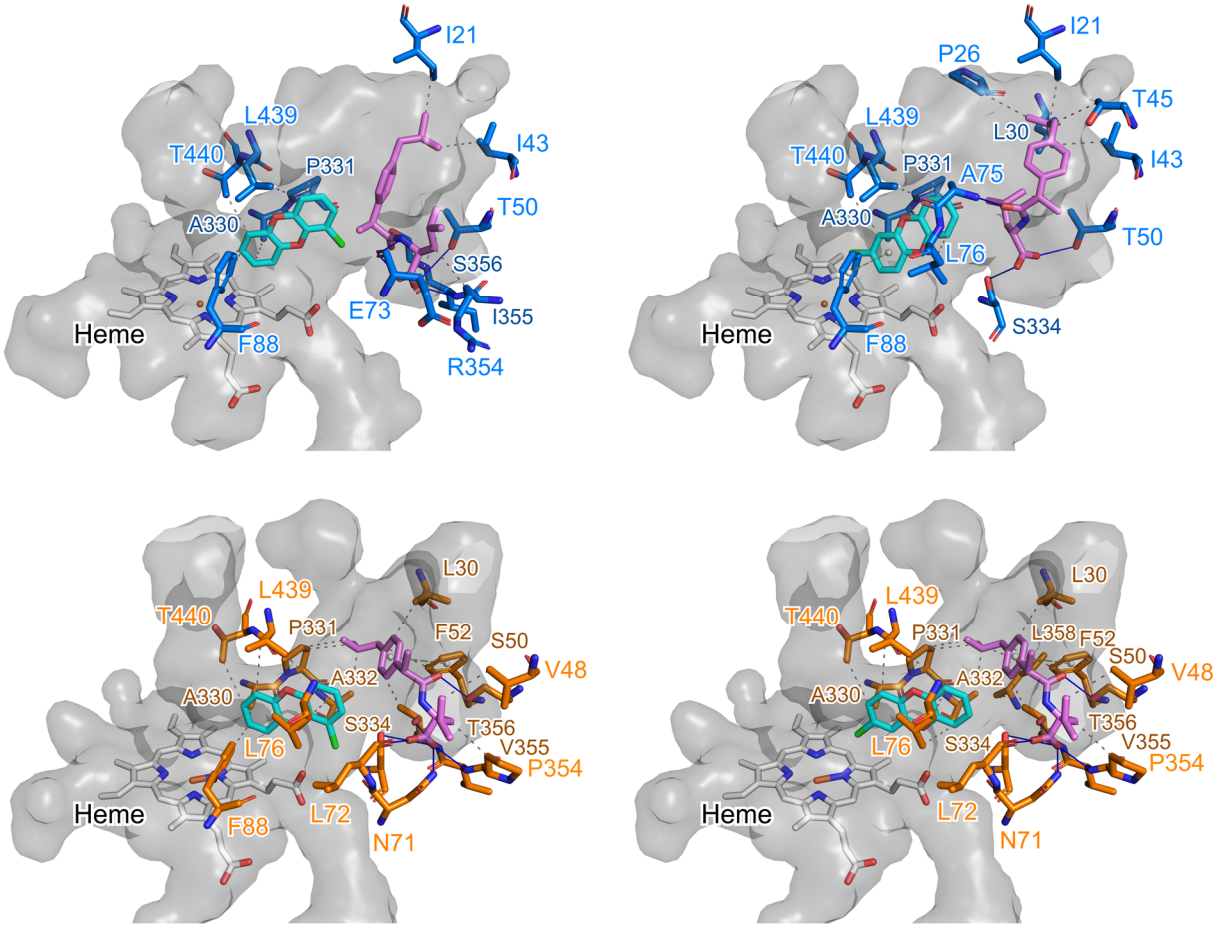

Fig. S11. Docking simulations of CDDs and (*S*)-Ibu-Leu with CYP102A2 and CYP102A3. The substrate (1- or 2-CDD) and (*S*)-Ibu-Leu were docked stepwise to the representative structures extracted from MD simulations, and protein-ligand interactions were analyzed and visualized using PLIP. Upper panels: CYP102A2; lower panels: CYP102A3. Left panels: 1-CDD; right panels: 2-CDD. Cyan: CDDs; magenta: (*S*)-Ibu-Leu.

References

1. K. Yonemura, S. Ariyasu, J. K. Stanfield, K. Suzuki, H. Onoda, C. Kasai, H. Sugimoto, Y. Aiba, Y. Watanabe and O. Shoji, *ACS Catal.*, 2020, **10**, 9136-9144.
2. Y. Yokoyama, S. Ariyasu, M. Karasawa, C. Kasai, Y. Aiba, H. Sugimoto and O. Shoji, *ChemCatChem*, 2025, **17**, e202401641.
3. M. Karasawa, J. K. Stanfield, S. Yanagisawa, O. Shoji and Y. Watanabe, *Angew. Chem. Int. Ed.*, 2018, **57**, 12264-12269.
4. J. Kabisch, A. Thürmer, T. Hübel, L. Popper, R. Daniel and T. Schweder, *J. Biotechnol.*, 2013, **163**, 97-104.
5. B.-M. Koo, G. Kritikos, J. D. Farelli, H. Todor, K. Tong, H. Kimsey, I. Wapinski, M. Galardini, A. Cabal, J. M. Peters, A.-B. Hachmann, D. Z. Rudner, K. N. Allen, A. Typas and C. A. Gross, *Cell Syst.*, 2017, **4**, 291-305.
6. J. Jumper, R. Evans, A. Pritzel, T. Green, M. Figurnov, O. Ronneberger, K. Tunyasuvunakool, R. Bates, A. Žídek, A. Potapenko, A. Bridgland, C. Meyer, S. A. A. Kohl, A. J. Ballard, A. Cowie, B. Romera-Paredes, S. Nikolov, R. Jain, J. Adler, T. Back, S. Petersen, D. Reiman, E. Clancy, M. Zielinski, M. Steinegger, M. Pacholska, T. Berghammer, S. Bodenstein, D. Silver, O. Vinyals, A. W. Senior, K. Kavukcuoglu, P. Kohli and D. Hassabis, *Nature*, 2021, **596**, 583-589.
7. F. Sievers, A. Wilm, D. Dineen, T. J. Gibson, K. Karplus, W. Li, R. Lopez, H. McWilliam, M. Remmert, J. Söding, J. D. Thompson and D. G. Higgins, *Mol. Syst. Biol.*, 2011, **7**, 539.
8. D. C. Bas, D. M. Rogers and J. H. Jensen, *Proteins:Struct., Funct., Bioinf.*, 2008, **73**, 765-783.
9. K. Shahrokh, A. Orendt, G. S. Yost and T. E. Cheatham, III, *J. Comput. Chem.*, 2012, **33**, 119-133.
10. W. L. Jorgensen, J. Chandrasekhar, J. D. Madura, R. W. Impey and M. L. Klein, *J. Chem. Phys.*, 1983, **79**, 926-935.
11. D. A. Case, H. M. Aktulga, K. Belfon, D. S. Cerutti, G. A. Cisneros, V. W. D. Cruzeiro, N. Forouzesh, T. J. Giese, A. W. Götz, H. Gohlke, S. Izadi, K. Kasavajhala, M. C. Kaymak, E. King, T. Kurtzman, T.-S. Lee, P. Li, J. Liu, T. Luchko, R. Luo, M. Manathunga, M. R. Machado, H. M. Nguyen, K. A. O'Hearn, A. V. Onufriev, F. Pan, S. Pantano, R. Qi, A. Rahnamoun, A. Risheh, S. Schott-Verdugo, A. Shajan, J. Swails, J. Wang, H. Wei, X. Wu, Y. Wu, S. Zhang, S. Zhao, Q. Zhu, T. E. Cheatham, III, D. R. Roe, A. Roitberg, C. Simmerling, D. M. York, M. C. Nagan and K. M. Merz, Jr., *J. Chem. Inf. Model.*, 2023, **63**, 6183-6191.
12. J. A. Maier, C. Martinez, K. Kasavajhala, L. Wickstrom, K. E. Hauser and C. Simmerling, *J. Chem. Theory Comput.*, 2015, **11**, 3696-3713.
13. J. Wang, R. M. Wolf, J. W. Caldwell, P. A. Kollman and D. A. Case, *J. Comput. Chem.*, 2004, **25**, 1157-1174.
14. M. R. Shirts, C. Klein, J. M. Swails, J. Yin, M. K. Gilson, D. L. Mobley, D. A. Case and E. D. Zhong, *J. Comput.-Aided Mol. Des.*, 2017, **31**, 147-161.
15. M. J. Abraham, T. Murtola, R. Schulz, S. Páll, J. C. Smith, B. Hess and E. Lindahl, *SoftwareX*, 2015, **1-2**, 19-25.
16. G. Bussi, D. Donadio and M. Parrinello, *J. Chem. Phys.*, 2007, **126**, 014101.
17. M. Bernetti and G. Bussi, *J. Chem. Phys.*, 2020, **153**, 114107.
18. M. Parrinello and A. Rahman, *J. Appl. Phys.*, 1981, **52**, 7182-7190.
19. T. Darden, D. York and L. Pedersen, *J. Chem. Phys.*, 1993, **98**, 10089-10092.
20. B. Hess, *J. Chem. Theory Comput.*, 2008, **4**, 116-122.
21. O. Trott and A. J. Olson, *J. Comput. Chem.*, 2010, **31**, 455-461.

22. S. Salentin, S. Schreiber, V. J. Haupt, M. F. Adasme and M. Schroeder, *Nucleic Acids Res.*, 2015, **43**, W443-W447.
23. D. R. Nelson, *Hum. Genomics*, 2009, **4**, 59.
24. D. Gront, K. Syed and D. R. Nelson, *Protein Sci.*, 2025, **34**, e70057.
25. K. Mansouri, C. M. Grulke, R. S. Judson and A. J. Williams, *J. Cheminf.*, 2018, **10**, 10.